Nitrate sources and transformation processes in groundwater of a coastal area experiencing various environmental stressors

Lamine Boumaiza[1], Safouan Ben Ammar[2], Romain Chesnaux[3], Randy L. Stotler[1], Bernhard Mayer[4], Frédéric Huneau[5], Karen H. Johannesson[6], Jana Levison[7], Kay Knöller[8], Christine Stumpp[9]

[1] University of Waterloo, Department of Earth and Environmental Sciences, Waterloo, Ontario, N2T 0A4, Canada

[2] Université de Carthage, Institut Supérieur des Technologies de l'Environnement de l'Urbanisme et de Bâtiment, Tunis, 2035, Tunisia

[3] Université du Québec à Chicoutimi, Département des Sciences Appliquées, Saguenay, Québec, G7H 2B1, Canada

[4] University of Calgary, Department of Geoscience, Calgary, Alberta, T2N 1N4 Canada

[5] Université de Corse, CNRS UMR 6134 SPE, Département d'Hydrogéologie, Campus Grimaldi BP52, Corte, 20250, France

[6] University of Massachusetts Boston, School for the Environment, Boston, Massachusetts, 02125, USA

[7] University of Guelph, School of Engineering, Morwick G360 Groundwater Research Institute, Guelph, Ontario, N1G 2W1, Canada

[8] Helmholtz Centre for Environmental Research, Department of Catchment Hydrology, Halle, Saale, 06120, Germany

[9] University of Natural Resources and Life Sciences, Institute of Soil Physics and Rural Water Management, Vienna, 1190, Austria

Abstract

In coastal salinized groundwater systems, contamination from various nitrate (NO_3) inputs combined with complex hydrogeochemical processes make it difficult to distinguish NO_3 sources and identify potential NO_3 transformation processes. Effective field-based NO_3 studies in coastal areas are needed to improve the understanding of NO_3 contamination dynamics in groundwater of such complex coastal systems. This study focuses on a typical Mediterranean coastal agricultural area, located in Tunisia, experiencing substantial NO_3 contamination from multiple anthropogenic sources. Here, multiple isotopic tracers ($\delta^{18}O_{H2O}$, $\delta^{2}H_{H2O}$, $\delta^{15}N_{NO3}$, $\delta^{18}O_{NO3}$, and $\delta^{11}B$) combined with a Bayesian isotope MixSIAR model are used (i) to identify the major NO_3 sources and their contributions, and (ii) to describe the potential NO_3 transformation processes. The measured NO_3 concentrations in groundwater are above the natural baseline threshold, suggesting anthropogenic influence. The measured isotopic composition of NO_3 indicates that manure, soil organic matter, and sewage are the potential sources of NO_3, while $\delta^{11}B$ values constrain the NO_3 contamination to manure; a finding that is supported by the results of MixSIAR model revealing that manure-derived NO_3 dominates over other likely sources. Nitrate derived from manure in the study area is attributed to organic fertilizers used to promote crop growth, and livestock that deposit manure directly on the ground surface. Evidence for ongoing denitrification in groundwaters of the study area is supported by an enrichment in both ^{15}N and ^{18}O in the remaining NO_3, although isotopic mass balances between the measured and the theoretical $\delta^{18}O_{NO3}$ values also suggest the occurrence of nitrification. The simultaneous occurrence of these biogeochemical processes with heterogeneous distribution across the study area reflect the complexity of interactions within the investigated coastal aquifer. The multiple isotopic tracer approach used here can identify the effect of multiple NO_3 anthropogenic activities in coastal environments, which is fundamental for sustainable groundwater resources management.

Keywords

Nitrate, Aquifer, Denitrification, Nitrification, Stable isotopes, MixSIAR

1 Introduction

Nitrate (NO_3) is a ubiquitous environmental contaminant that is primarily associated with anthropogenic activities, with limited contributions from natural geological and atmospheric sources in most areas (Hendry et al., 1984; Holloway and Dahlgren, 2002; Scanlon et al., 2008). NO_3 concentrations in groundwater systems above the maximum drinking water concentration of 50 mg/L (WHO, 2017) have been observed in numerous countries with industrial agriculture. Example of aquifers with elevated groundwater NO_3 concentrations include the Mediterranean coastal aquifer of Taleza in Algeria with concentrations of up to 230 mg/L (Boumaiza et al., 2020), the Córdoba aquifers in Argentina with concentrations of up to 500 mg/L (Blarasin et al., 2014), the Weining groundwater system in China with concentrations of up to 800 mg/L (He et al., 2022), and the Noyil river basin aquifer in India in which NO_3 concentrations to up to 1,500 mg/L are reported (Jacks and Sharma, 1983). These and several other studies focussed on groundwater NO_3 contamination due to the adverse effects of NO_3 on both human and environmental health. For example, long-term consumption of excessive NO_3 in drinking water increases methemoglobinemia in infants (blue baby syndrome), and spontaneous abortion, thyroid disorders, colorectal and stomach cancer, and neural tube defects in adults (Schroeder et al., 2020; Ward et al., 2018). The discharge of NO_3 into surface water bodies causes eutrophication of freshwater and marine environments, leading to considerable reduction of aquatic life and biodiversity (Brookfield et al., 2021; Gomez Isaza et al., 2020; Yeshno et al., 2019). Incomplete denitrification of NO_3 in aquifer systems leads to the formation and release of nitrous oxide gas (N_2O), which is a powerful greenhouse gas contributing to global climate change (Sutton et al., 2011; Weeks and McMahon, 2007).

Dissolved NO_3 can also oxidize and mobilize heavy metals such as uranium and selenium (Mills et al., 2016; Moon et al., 2007).

Worldwide population growth has introduced an increased level of anthropogenic activities in rural and developing areas. Excessive use of synthetic and organic fertilizers in agricultural fields to promote crop growth contribute up to 80% of the worldwide reactive produced nitrogen and releases NO_3 to groundwater (Lasagna and De Luca, 2017; Pulido-Bosch et al., 2018). In developing urban areas, NO_3 can be transported to groundwater by wastewater discharge from inefficient private sanitation systems and sewer systems (Boumaiza et al., 2020; Matiatos, 2016; Puig et al., 2017; Vystavna et al., 2017). The level of NO_3 contamination and its fate in groundwater systems not only depends on the type and intensity of anthropogenic activities, but also on the structure and hydrogeological characteristics of affected aquifers. In coastal aquifers, it is particular challenging to study the sources and fate of groundwater NO_3 contamination because seawater intrusion, induced by and human activities and sea level rise due to climate change (Chesnaux et al., 2021; Lao et al., 2022b), can lead to mutually interacting sources and geochemical processes (Boumaiza et al., 2020; Elmeknassi et al., 2022). In addition, elevated NO_3 concentration in groundwater can fuel a number of complex geochemical reactions (Re et al., 2021; Re and Sacchi, 2017). Therefore, field-based NO_3 studies in coastal aquifers are needed to improve the understanding of NO_3 contamination in such complex hydrogeological systems.

Stable isotopic tracers have been widely used to investigate groundwater NO_3 contamination sources and processes. The stable isotopes of nitrate ($\delta^{15}N_{NO3}$ and $\delta^{18}O_{NO3}$) constitute a powerful tool not only for distinguishing NO_3 sources, but also for assessing

114 the biogeochemical processes that govern NO_3 cycling and persistence within groundwater
115 systems (Blarasin et al., 2020; Boumaiza et al., 2022a; Lane et al., 2020; Zendehbad et al.,
116 2019). However, isotopic signatures of some NO_3 sources overlap, and processes such as
117 nitrification, denitrification, and ammonia volatilization can change NO_3 concentrations
118 and modify $\delta^{15}N_{NO3}$ and $\delta^{18}O_{NO3}$ values, masking the isotopic signature of the original NO_3
119 sources (Jin et al., 2015; Kendall et al., 2007). Thus, additional isotope tracers (e.g., $\delta^{11}B$,
120 $^{87}Sr/^{86}Sr$, and $\delta^{34}S$) and statistical Bayesian models (e.g., MixSIAR) have also been used,
121 separately or combined with the stable isotope composition of NO_3 to efficiently track NO_3
122 sources and quantify their relative contributions (Boumaiza et al., 2022b; Erostate et al.,
123 2018; Kaown et al., 2023; Kruk et al., 2020). Hence, multi-isotope approaches are
124 promising tools for identifying the NO_3 sources and evaluating the fate of NO_3 within
125 groundwater systems.

126 One of the coastal groundwater systems, underlying an important economically
127 strategic agricultural area, is the plain of Oussja-Ghar-Melah (OGM) in Tunisia. This
128 groundwater system is located along the Mediterranean coast where groundwater resources
129 are heavily affected by multiple anthropogenic sources of NO_3 that contribute to
130 deteriorating groundwater quality, and is also at risk from seawater intrusion owing to
131 overexploitation of local groundwater resources (Carrubba, 2017; Ben Ammar et al., 2016).
132 The OGM system is subject to complex hydrogeochemical processes that can impact the
133 fate of NO_3 within the aquifer. Moreover, the Ghar-El-Melh Lagoon (GEM Lagoon), which
134 was designated a UNESCO-Ramsar ecological site (No.1706) in 2007 is located down
135 hydrologic gradient from the OGM aquifer system emphasizing the international
136 importance of the study area. Previous groundwater quality investigations within the OGM

plain chiefly focused on assessing groundwater salinization and only hypothesized potential NO_3 sources (Ben Ammar et al., 2016; Bouzourra et al., 2015). A detailed investigation of groundwater NO_3 contamination and potential transformation processes affecting NO_3 in the aquifer underlying the OGM plain have not yet been conducted. Therefore, the main objectives of this study are: (i) to identify the dominant anthropogenic sources of NO_3 and distinguish potential NO_3 transformation processes within the OGM groundwater system by combining multiple stable isotope tracers ($\delta^{18}O_{H2O}$, $\delta^{2}H_{H2O}$, $\delta^{15}N_{NO3}$, $\delta^{18}O_{NO3}$, and $\delta^{11}B$); (ii) to quantify the contributions of different NO_3 sources by using a Bayesian isotope mixing model (MixSIAR); and (iii) to identify the potential NO_3 transformation processes. Ultimately, the outcomes of this study will help local groundwater managers to develop sustainable environmental management strategies for the OGM plain; and inform future studies of the many Mediterranean coastal systems with similar environmental stresses.

2 Description of the study area

2.1 Geographic location and climate

The study area of the OGM is a coastal agricultural plain located at the border of the Provinces of Bizerte and Ariana in northeastern Tunisia (Figure 1). The study area is surrounded from the southwest to the northeast by a series of discontinuous mountains (i.e., Menzel Ghoul, Kechabta, and Nadhour) varying in altitude from 300 to 400 m above sea level. Towards the south, the OGM plain is an open and flat valley system belonging to the Medjerda paleodelta. The northeast-southeast boundary of the study area constitutes the GEM Lagoon, which is connected to the Mediterranean Sea (Figure 1). The study area covers a surface of about 60 km^2, with topography characterized by a slight downslope

160 from the hinterland in the southwest towards the Mediterranean Sea in the east and
161 northeast (Ben Ammar et al., 2016). Several large rural villages are located in the study
162 area including Ghar-El-Melh to the northeast, Zouaouine and Gournata to the southwest,
163 and Oussja within the center of the plain. Between these population centers are many
164 smaller rural communities.

165 The climate of the study area is subhumid Mediterranean with two distinct periods:
166 (i) a wet period, occurring from October to April, with a monthly average temperature of
167 11 °C; and (ii) a dry period, occurring from May to September, with a monthly average
168 temperature of 27 °C (Ben Ammar et al., 2016). The OGM region captures an average
169 annual precipitation amount of about 500 mm with 90% occurring during the wet period
170 (Ben Ammar et al., 2016). The assessed mean annual potential evapotranspiration is
171 estimated to be ~1,350 mm, clearly indicating a deficient annual water budget for the study
172 area. Nevertheless, the excess of meteoric precipitation during the wet period provides
173 potential for aquifer recharge (Ben Ammar et al., 2016; Bouzourra et al., 2015).

174 ## 2.2 **Geology**

175 The study area belongs to a tectonic depression that filled with clastic sediments following
176 a major Mio-Pliocene subsidence. This depression was previously invaded by a postglacial
177 marine transgression, developing a marine paleoenvironment; after which the depression
178 gradually infilled with fluvial deposits (i.e., sand, silt, and clay) initially transported by the
179 Medjerda River (Burrolet and Dumon, 1952; Pimienta, 1959). The study area thus evolved
180 from a marine lagoon into a coastal evaporitic basin, in which the GEM Lagoon represents
181 the current remnant of the Utique paleoshoreline (Bouzourra et al., 2015). The aquifer

182 under the plain of OGM is comprised of granular material provided by the Late-
183 Pliocene/Quaternary deposition.
184

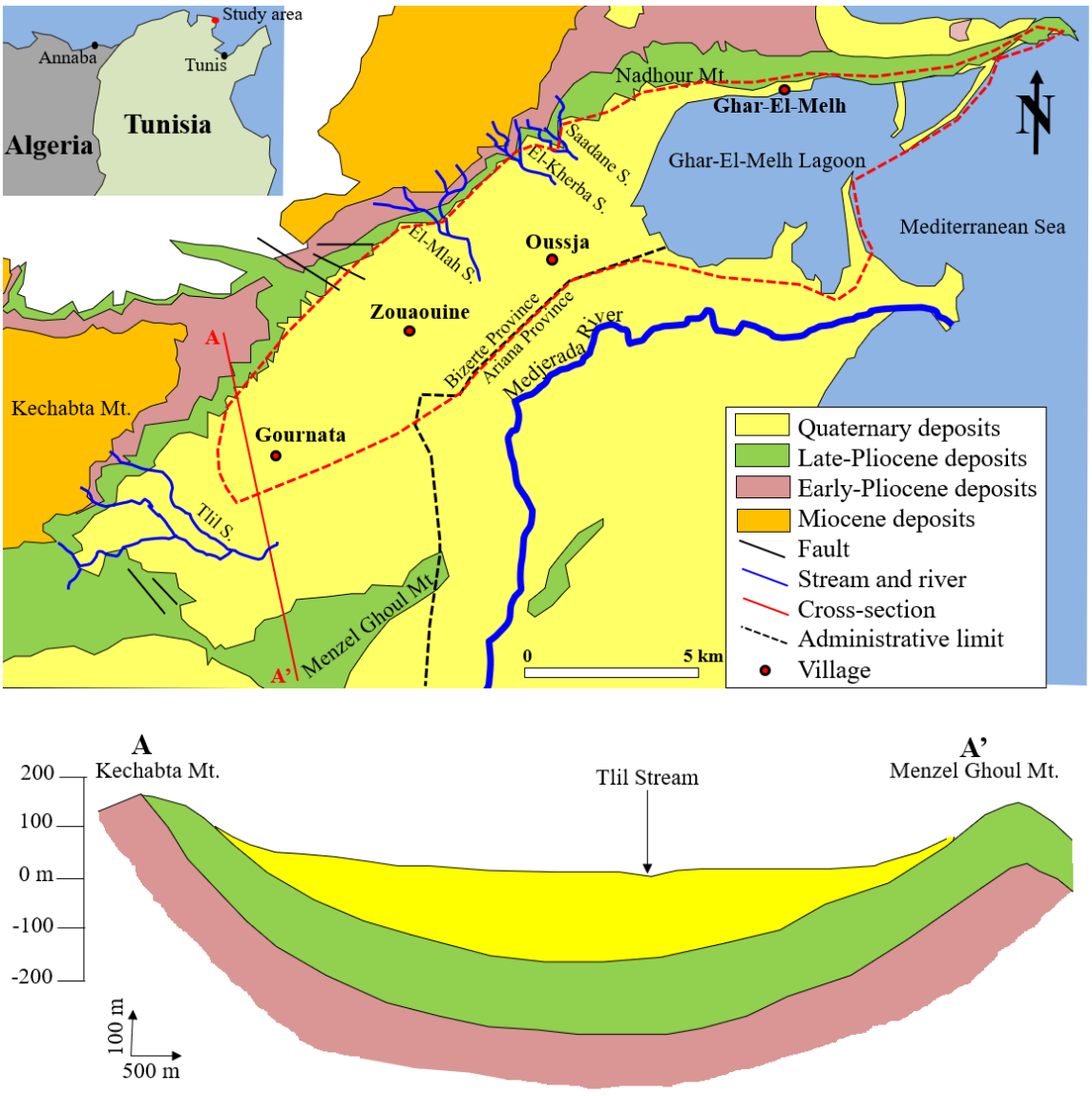

185
186
187
188 Figure 1. Simplified geology of surface deposits over the plain of OGM region, and
189 schematic cross-section AA' through the study area (adapted from Burrolet and Dumon,
190 1952; Melki et al., 2011). In dashed red is the approximate limit of the study area. Only the
191 permanent streams are indicated in this figure.
192
193

194 Geophysical Seismic reflection investigations demonstrated that the thickness of
195 the Plio-Quaternary deposits varies from 300 m at the southwest sector of the study area to
196 >600 m in the northeast (Melki et al., 2011). The granular Plio-Quaternary deposits
197 unconformably rest on Mio-Pliocene sequence that consists of clay, marl, and gypsum,
198 which outcrops in the surrounding mountains (Figure 1). Miocene rocks are covered in
199 some places by clay material attributed to the Early Pliocene (Burrolet and Dumon, 1952;
200 Chelbi et al., 1995). A ~300 m thick Late-Pliocene formation (Porto Farina formation)
201 overlies the impervious Miocene and Early Pliocene units, and is mainly composed of sand
202 and sandstone with clays intercalations (Burrolet and Dumon, 1952; Melki et al., 2011).

203 2.3 **Hydrogeological background**

204 The OGM plain overlies an unconfined heterogeneous granular aquifer with a thickness of
205 up to 100 m (Ben Ammar et al., 2016). This aquifer is mainly recharged by direct
206 precipitation, runoff from the surrounding mountains, and by several permanent streams
207 including the Saadane, El-Kherba, and El-Melah streams in the north, and Tlil stream in
208 the southwest, all of which are sourced from the surrounding mountains. These streams
209 drain small catchment areas ranging from 6 to 17 km^2 (Saadaoui, 1983). The water table in
210 the aquifer varies between 2 and 24 m depth below the ground surface, and groundwater
211 generally flows northeastward towards the GEM Lagoon and Mediterranean Sea (Ben
212 Ammar et al., 2016). The chemistry of groundwater within the OGM aquifer is dominated
213 by chloride-water type, i.e., (Na, Ca)-Cl-rich, which are hypothesized to reflect multiple
214 hydrogeochemical processes including dissolution/precipitation of carbonate minerals,
215 dissolution of gypsum and halite, and cation exchange (Ben Ammar et al., 2016; Bouzourra

et al., 2015). Groundwater salinization is thought to be the result of seawater intrusion and the deposition of seawater aerosols flushing into the subsurface (Ben Ammar et al., 2016).

The OGM aquifer system is considered to be vulnerable to the contamination with three levels based on the DRASTIC index (Ouerghi, 2021). These are as follows: (i) a zone with low vulnerability to contamination, representing 28% of the study area, and located in the northeastern portion of the study area proximal to Ghar-El-Melh village; (ii) a second zone, occupying the center of the study area (45%) close to Oussja and Zouaouine villages with an average vulnerability level; and (iii) a third zone with very high vulnerability level (27%) located in the southwestern part of the study area (around Gournata).

2.4 **Land use and anthropogenic contamination**

The earliest first settlements in the study area include the large villages of Ghar-El-Melh in the northeast, Zouaouine and Gournata in the southwest, and Oussja in the center of the plain (Figure 1). Subsequently, several small rural communities developed throughout the study area with an approximate combined population of 19,000 permanent inhabitants. The rural communities in the study area are connected to a potable water supply via a pipeline-system provided by SONEDE (*Société Nationale d'Exploitation et de Distribution des Eaux*). However, only 60% of the rural sectors, including the large villages of Ghar-El-Melh and Oussaja, are connected to a sewage network, which has only operated since 2010. Before 2010, all the communities used private septic tank systems.

Despite increased urbanization across the study area, agricultural fields still dominate the land use (~80%). Agricultural activities (i.e., production of various vegetables in open agricultural fields) are supported by irrigation using surface waters from three following sources: (i) the Medjerda River located at the south of the study area, (ii) an

239 artificial drainage network operated since 1990 over the central part of the study area, and
240 (iii) a series of small dams installed at the edges of the surrounding mountains to the north.
241 In addition, there is a large number of shallow hand-dug wells (~1,500 wells) in the study
242 area that are used to obtain groundwater for irrigating the agricultural fields (Ben Ammar
243 et al., 2016; Bouzourra et al., 2015).

244 The effect of both agriculture and urban development resulted in a deterioration of
245 groundwater quality with regards to nitrate concentrations (Bouzourra et al., 2015;
246 Ouerghi, 2021). Reported groundwater NO_3 concentrations ranged from 5 to 150 mg/L,
247 with elevated NO_3 concentrations coinciding with locations of intense urbanization and
248 agricultural activities (Ben Ammar et al., 2016; Bouzourra et al., 2015). These researchers
249 suggested that organic/synthetic fertilizers used for agriculture, livestock (i.e., cattle for
250 dairy and meat production) manure, and septic tanks constituted the major sources of NO_3
251 (Ben Ammar et al., 2016; Bouzourra et al., 2015; Carrubba, 2014). However, clear
252 evidence demonstrating the sources of the groundwater NO_3 contamination has not been
253 reported. Increasing demand for irrigation water has generated substantial groundwater
254 exploitation reaching 13 million cubic meters per year (in 2009), which is roughly 2-fold
255 higher than the annual aquifer recharge (Ben Ammar et al., 2016; Bouzourra et al., 2015;
256 MAT, 2006). Hence, overexploitation of groundwater led to drop in elevation of the water
257 table within the OGM aquifer that has subsequently supported seawater intrusion in some
258 locations, along groundwater salinization to as much as 3,000 mg/L for total dissolved
259 solids (Ayache et al., 2009; Bouchouicha, 2004; Bouzourra et al., 2015).

260 # 3 Material and methods

261 ## 3.1 Sampling network and protocol

A single comprehensive water sampling campaign was carried out through the period ranging from October 19 to November 2 of 2022. The sampling campaign included 21 groundwater samples collected over the entire study area and 2 surface water samples, one each collected from the GEM Lagoon and the Mediterranean Sea (Figure 2). Groundwater samples were collected from shallow irrigation wells having 2-3 m diameters, with a static groundwater depth of 2-20 m below the ground surface. Prior to sampling, stagnant groundwater present in the wells was purged using a pumping system. During pumping the physico-chemical parameters (temperature (T), pH, total dissolved solids (TDS), electrical conductivity (EC), and dissolved oxygen (DO)) of the pumped groundwater were monitored using a calibrated portable multiparameter probe (Lange sensION 156 Hach Instrument), until stabilized within ±10%. Groundwater was then collected at the discharge pipe of the pumping system.

During fieldwork, the water samples for major ion analyses were filtered using 0.45-μm nitrocellulose membrane filters attached to 100-mL luer-lock syringe samplers, before being poured in two separate 40-mL amber bottles. Cation samples were acidified to pH <2 by adding 2-3 drops of ultrapure nitric acid (HNO_3) to prevent major cation precipitation or adsorption during storage. The samples for $\delta^{2}H_{H2O}$ and $\delta^{18}O_{H2O}$ analyses were collected in 25-mL amber bottles, whereas those for $\delta^{15}N_{NO3}/\delta^{18}O_{NO3}$, and $\delta^{11}B$ analyses were filtered into 50-mL and 250-mL polyethylene bottles, respectively. All water samples were collected in bottles without headspace and closed with caps containing Teflon septa parafilm to prevent evaporation. For suitable climate and safe storage conditions, all water samples were temporarily stored in a portable cooler before being transferred further to a refrigerator for storage at 4°C at the completion of the fieldwork

day until analysis. The samples collected for isotopic analysis of NO_3 were frozen to avoid variations caused by biological processes until the targeted isotopic analyses were performed in the laboratory.

3.2 Laboratory chemical and stable isotope analyses

Chemical analyses (HCO_3^-, Br^-, NO_3^-, Cl^-, K^+, Mg^{2+}, NH_4^+, Na^+, Ca^{2+} and SO_4^{2-}) were performed at the Laboratory for Inorganic and Organic Chemistry of the Technical University of Darmstadt (Germany). HCO_3 concentrations were determined using Alkalinity Checker® (HI775, Hanna Instruments, Woonsocket, USA), whereas the other ion concentrations were determined using a Metrohm 882 Compact Ion Chromatograph plus equipped with a Metrosep A Supp 5-250 column for anions and a Metrosep C 4-250 column for cations (Metrohm, Herisau, Switzerland). The water stable isotope (δ^2H_{H2O} and $\delta^{18}O_{H2O}$) analyses were completed at the Laboratory of the Institute of Soil Physics and Rural Water Management in Vienna (Austria). These isotopic values were measured using a laser-based isotope analyzer (Picarro L2140-*i*) according to the analytical scheme recommended by the International Atomic Energy Agency (IAEA) (Penna et al., 2010). Nitrate stable isotope ($\delta^{15}N_{NO3}$ and $\delta^{18}O_{NO3}$) analyses were completed at the Helmholtz Center for Environmental Research in Halle/Saale (Germany), using the denitrifier method with bacteria strains of *Pseudomonas chlororaphis* (ATCC #13985 equal to DSM-6698) according to the protocols recommended by Casciotti et al. (2002) and Sigman et al. (2001).

Boron (B) concentrations and $\delta^{11}B$ values in water samples were both analyzed at the Isotope Science Laboratory of the University of Calgary (Alberta, Canada). Concentrations of dissolved boron in groundwater were measured using a Varian 725 inductively coupled plasma-optical emission spectrometer (ICP-OES) with a measurement

uncertainty ±2%, whereas $\delta^{11}B$ values were measured using a Neptune Multi-Collector Inductively Coupled Plasma Mass Spectrometer (MC-ICP-MS) (Thermo Scientific) according to the analytical schemes recommended by Guerrot et al. (2011) and Gaillardet et al. (2001) depending on the B concentration of the samples. The isotope values, expressed in per mil (‰) using delta (δ) notation, were calculated using Equation 1, in which R_{sample} and $R_{standard}$ are the sample and the international reference standard values of the heavier to the lighter isotope, respectively (i.e., $^{2}H/^{1}H$, $^{18}O/^{16}O$, $^{15}N/^{14}N$, or $^{11}B/^{10}B$).

$$\delta = \frac{R_{sample} - R_{standard}}{R_{standard}} \quad (1)$$

The international reference standards relative to which the sample isotopic values are reported are the Vienna Mean Standard Ocean Water (VSMOW) for $\delta^{2}H_{H2O}$, $\delta^{18}O_{H2O}$ and $\delta^{18}O_{NO3}$, and atmospheric nitrogen (AIR) for $\delta^{15}N_{NO3}$. The precision of the analytical instrument was generally better than ±0.3‰ for $\delta^{2}H_{H2O}$ and ±0.1‰ for $\delta^{18}O_{H2O}$, whereas the reproducibility for the $\delta^{15}N_{NO3}$ and the $\delta^{18}O_{NO3}$ measurements were ±0.6‰ and ±0.4‰, respectively. The isotope measurements of $\delta^{11}B$ had a mean precision of ±2‰, which was determined following a replicate analysis of standards and samples. In the present study, the $\delta^{18}O_{H2O}$ and $\delta^{2}H_{H2O}$ values are interpreted according to the Global Meteoric Water Line (GMWL) (Craig, 1961) and the Western Mediterranean Meteoric Water Line (WMMWL) (Celle, 2000). The deuterium excess (d-excess = $\delta^{2}H - 8\delta^{18}O$), which represents the enrichment in $\delta^{2}H_{H2O}$ exceeding that of $\delta^{18}O_{H2O}$ occurring principally during evaporation, is an indicator of kinetic fractionation and used to assess the evaporation effect over mixing where a d-excess <10‰ is indicative of the evaporation effect, otherwise, mixing with continental runoff is suggested (Dansgaard, 1964).

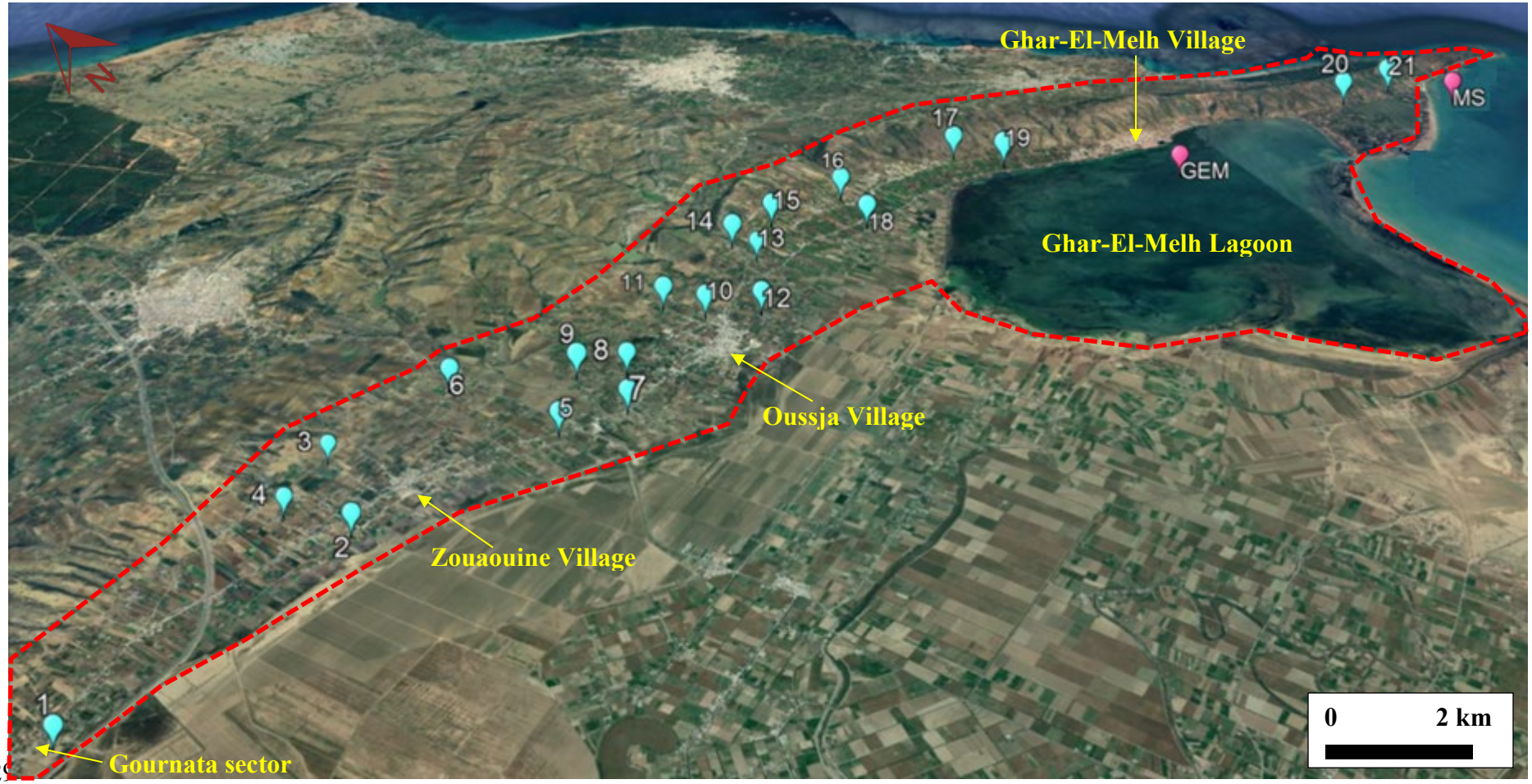

Figure 2. Perspective overview of study area (Google Earth) with location of groundwater samples and surface water samples collected over the study area. Groundwater sampling sites are indicated with numbers 1 to 21, whereas surface water samples are GEM (Ghar-El-Melh Lagoon) and MS (Mediterranean Sea). The red dashed line is the approximate limit of the study area including the GEM Lagoon.

3.3 **Nitrate sources determination, apportionment, and transformation**

To identify the predominant NO_3 sources in water samples, the $\delta^{15}N_{NO3}$ versus $\delta^{18}O_{NO3}$ diagram (Kendall, 1998) is used. This diagram provides zones of isotopic compositions that correspond to specific sources of NO_3, which include atmospheric precipitation (AP), NO_3 based synthetic fertilizers (NOF), sewage and manure (S&M), NO_3 that is formed from nitrification of NH_4-fertilizers (NHF), or soil organic nitrogen (SON). To identify the occurrence of nitrification, an isotopic mass balance ($\Delta\delta^{18}O_{NO3}$) between the measured $\delta^{18}O_{NO3}$ and the theoretical $\delta^{18}O_{NO3}$ is calculated. The theoretical $\delta^{18}O_{NO3}$ is evaluated by using Equation 2 (Aravena and Mayer, 2010), where $\delta^{18}O_{H2O}$ represents the measured oxygen groundwater stable isotope ratio and $\delta^{18}O_{O2}$ is the isotopic ratio of atmospheric oxygen assumed in equilibrium with a constant value of +23.5‰ (Aravena and Mayer, 2010; Blarasin et al., 2020; Moore et al., 2006). The contribution of NO_3 derived from nitrification process is calculated as a portion of the theoretical $\delta^{18}O_{NO3}$ to the measured $\delta^{18}O_{NO3}$ (Torres-Martínez et al., 2021).

$$\delta^{18}O_{NO3\ (theoretical)} = \left(\frac{2}{3}\ \delta^{18}O_{H2O}\right) + \left(\frac{1}{3}\ \delta^{18}O_{O2}\right) \quad (2)$$

Other diagrams and a Bayesian isotope model are used to distinguish between sewage and manure sources affecting groundwater contamination. Here, a diagram comparing B concentrations and $\delta^{11}B$ values and a plot of $\delta^{15}N_{NO3}$ versus $\delta^{11}B$ values are used. Both of these diagrams provide distinct zones for manure and sewage, thus providing a means to differentiate between manure and sewage sources (Komor, 1997; Puig et al., 2017; Vengosh et al., 1994). The MixSIAR model (Parnell et al., 2010) is used to quantify the proportional contributions of the identified NO_3 sources in the groundwater system.

The framework of Bayesian stable isotope mixing model is presented in Supplementary Text S1. More detail on the MixSIAR model development can be found in Stock et al. (2018). The inputs for the MixSIAR model are the $\delta^{15}N_{NO3}$ and $\delta^{11}B$ values measured in groundwater samples and the different $\delta^{15}N_{NO3}$ and $\delta^{11}B$ end-member isotopic values of the sources of nitrate. Here, the $\delta^{15}N_{NO3}$ and $\delta^{11}B$ end-members are adopted from Kaown et al. (2023), who investigated NO_3 contamination in an area with comparable anthropogenic sources. The isotope fractionation effect is not considered as the isotope data represent one current-state corresponding to one sampling campaign (i.e., no-variable states). Therefore, the isotopic fractionation effect in the MixSIAR model is set to zero similar to other studies (e.g., Cao et al., 2022; Kou et al., 2021).

4 Results

4.1 Chemical and isotopic composition of water

The chemical and isotopic results for the groundwater samples as well as the surface water samples collected from the GEM Lagoon and the Mediterranean Sea are listed in the Supplementary Table S1. Groundwater samples collected from the study area are slightly alkaline with pH values varying from 7.05 to 7.63. The measured EC values range between 1,272 and 7,980 µS/cm, whereas the TDS values vary from 630 to 4,280 mg/L reflecting the existance of fresh to brackish waters within the OGM aquifer. Excessive groundwater concentrations are revealed for SO_4 for 15% of groundwater samples, with a maximum of 667 mg/L and a median of 199 mg/L, relative to the respective drinking water limit of 500 mg/L that is recommended by the World Health Organization (WHO, 2017). The concentrations of HCO_3 are measured with a maximum of 265 mg/L and median value about 95 mg/L. High concentrations are identified for the other major elements including

Cl (max. = 2,338 mg/L, median = 602 mg/L), Na (max. = 1,400 mg/L, median = 325 mg/L), K (max. 47 mg/L, median = 7 mg/L), Mg (max. 168 mg/L, median = 60 mg/L), and Ca (max. 496 mg/L, median = 253 mg/L). The isotopic compositions of the groundwater samples range from −5.7‰ to −4.1‰ for $\delta^{18}O_{H2O}$ and from −32.1‰ to −24.3‰ for $\delta^{2}H_{H2O}$, with *d*-excess values ranging from +8 to +15‰ with a median value of +12‰. The GEM Lagoon sample has the highest $\delta^{18}O_{H2O}$ and $\delta^{2}H_{H2O}$ values (+1.4‰ and +9.7‰, respectively) and is comparable to the sample from the Mediterranean Sea (+1.3‰ and +9.5‰, respectively). These saline surface water samples, with TDS ranging from 33,000 to 39,000 mg/L, are enriched in ^{2}H and ^{18}O compared to groundwater samples and exhibit a low *d*-excess value (−1.1‰).

4.2 **Distribution of nitrate across the study area**

NO_3 concentrations in groundwater samples range from 4 to 489 mg/L, with an average of 132 mg/L (*n*=21). Surface water samples from the GEM Lagoon and the Mediterranean Sea have NO_3 concentrations of 87 and 104 mg/L, respectively (Supplementary Table S1). The distribution of NO_3 concentrations throughout the study area (Figure 3) shows two groundwater samples (#1 and #21) with NO_3 concentrations <10 mg/L located at the boundaries of the study area. Sample #1 is from the southwestern portion of the study area (sector of Gournata), whereas sample #21 is from the northeastern part of the study area (sector of Ghar-El-Melh village). The most recent previously available groundwater quality data are from Ben Ammar et al. (2016), who conducted groundwater sampling campaign in 2010 from pumping wells with comparable sampling protocol but different sampling wells. In 2010, NO_3 concentrations in groundwater from boundaries of the study area (i.e., sector of Gournata and Ghar-El-Melh village) were measured at 43 and 38 mg/L,

402 respectively (Ben Ammar et al., 2016). Groundwater samples most affected by NO_3 were
403 observed in 2010 within the sectors of Oussja and Zouaouine, with maximum NO_3
404 concentration of 136 mg/L (Ben Ammar et al., 2016). This is consistent with observation
405 from the present study, as elevated NO_3 concentrations are observed in these sectors of
406 Oussja and Zouaouine, but with a maximum of 378 mg/L (at sampling well #8).
407 Accordingly, the measured maximum NO_3 concentration in Oussja/Zouaouine sector in
408 2022 is over two times higher than the NO_3 concentration measured in 2010. In the
409 Oussja/Zouaouine area, there is a high number of wells supplying groundwater with
410 elevated NO_3 concentrations >150 mg/L (Figure 3), suggesting the existence of major and
411 permanent sources of NO_3 affecting groundwater. The highest NO_3 concentration (489
412 mg/L) is observed in the groundwater sample #17 collected between Ghar-El-Melh and
413 Oussja village at a location dominated by agricultural activities and surrounded by multiple
414 individual residences.

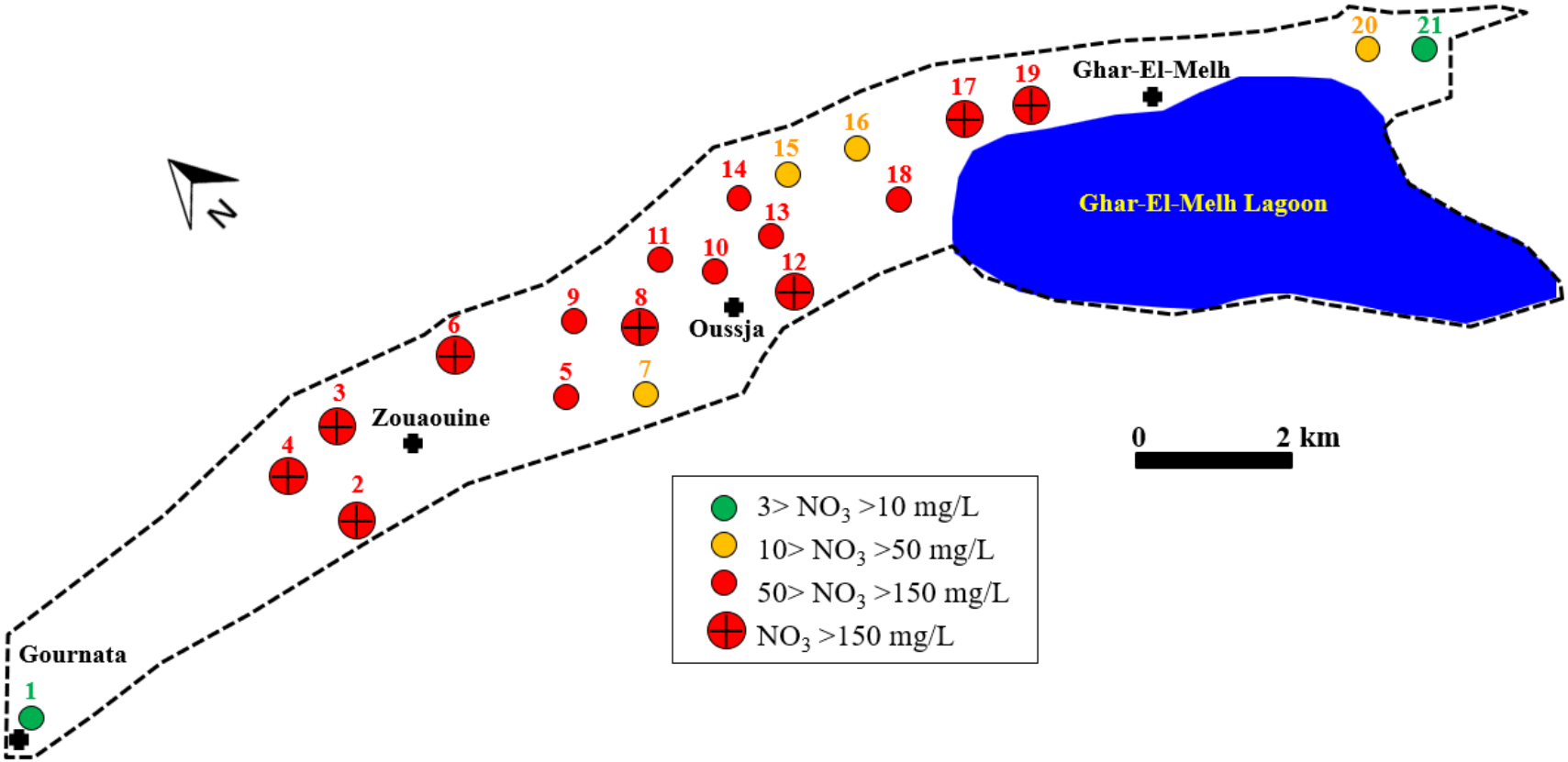

415 Figure 3. Spatial distribution of NO_3 concentrations in groundwater throughout the study area.

4.3 **Isotopic compositions of nitrate and boron and sources of nitrate**

The $\delta^{15}N_{NO3}$ values in groundwater range from +4.7 to +13.7‰ with a median value of +7.1‰, and $\delta^{18}O_{NO3}$ values vary between +4.1 and +15.6‰ with a median value of +7.5‰ (Supplementary Table S1). These median values are consistent with the range (4.9-11‰ and 5.7-12‰, respectively) of NO_3 isotopic compositions observed in other North-African coastal studies (Boumaiza et al., 2022a, 2022b, 2020; Re et al., 2021). The measured $\delta^{11}B$ values in groundwater samples range from +12.4 to +42.9‰, whereas in the GEM Lagoon and Mediterranean Sea they are +42.3 and +41.4‰, respectively (Supplementary Table S1). All groundwater samples (n=20) plot within the manure and sewage field of the Kendal diagram (Figure 4a), suggesting that manure and human wastewater are the main sources of NO_3 to local groundwater. However, 14 samples have NO_3 isotopic compositions that overlap with NO_3 from soil-derived nitrogen (Figure 4a). Boron isotope data indicate that manure is the principal source of NO_3 for most of the groundwater samples (18 out of 20) as well as the GEM Lagoon and the Mediterranean Sea (Figures 4b, c). The two remaining groundwater samples (#6 and #11) likely derive their NO_3 from mineral fertilizer (Figure 4b, c).

In the MixSIAR model, four NO_3 sources are selected including manure (M), sewage (S), soil organic nitrogen (SON) that are selected based on Figure 4a; and mineral fertilizer (NO_3 based fertilizers: NOF) that is selected based on Figure 4b, c. The assigned $\delta^{15}N_{NO3}$ end-members are 15.3±0.1‰ for M, 14.3±2.0‰ for S, −0.6±4.1‰ for SON, and 0.9±2.0‰ for NOF, whereas the $\delta^{11}B$ end-members are 33.1±2.1‰ for M, 5.4±2.7‰ for S, −2.6±1.9‰ for SON, and 2.0±1.0‰ for NOF (Kaown et al., 2023). MixSIAR results

reveal that manure is the primary source of NO_3 (60.4%), followed by NOF (19.1%), SON (16.1%), and sewage (4.3%) (Figure 4d).

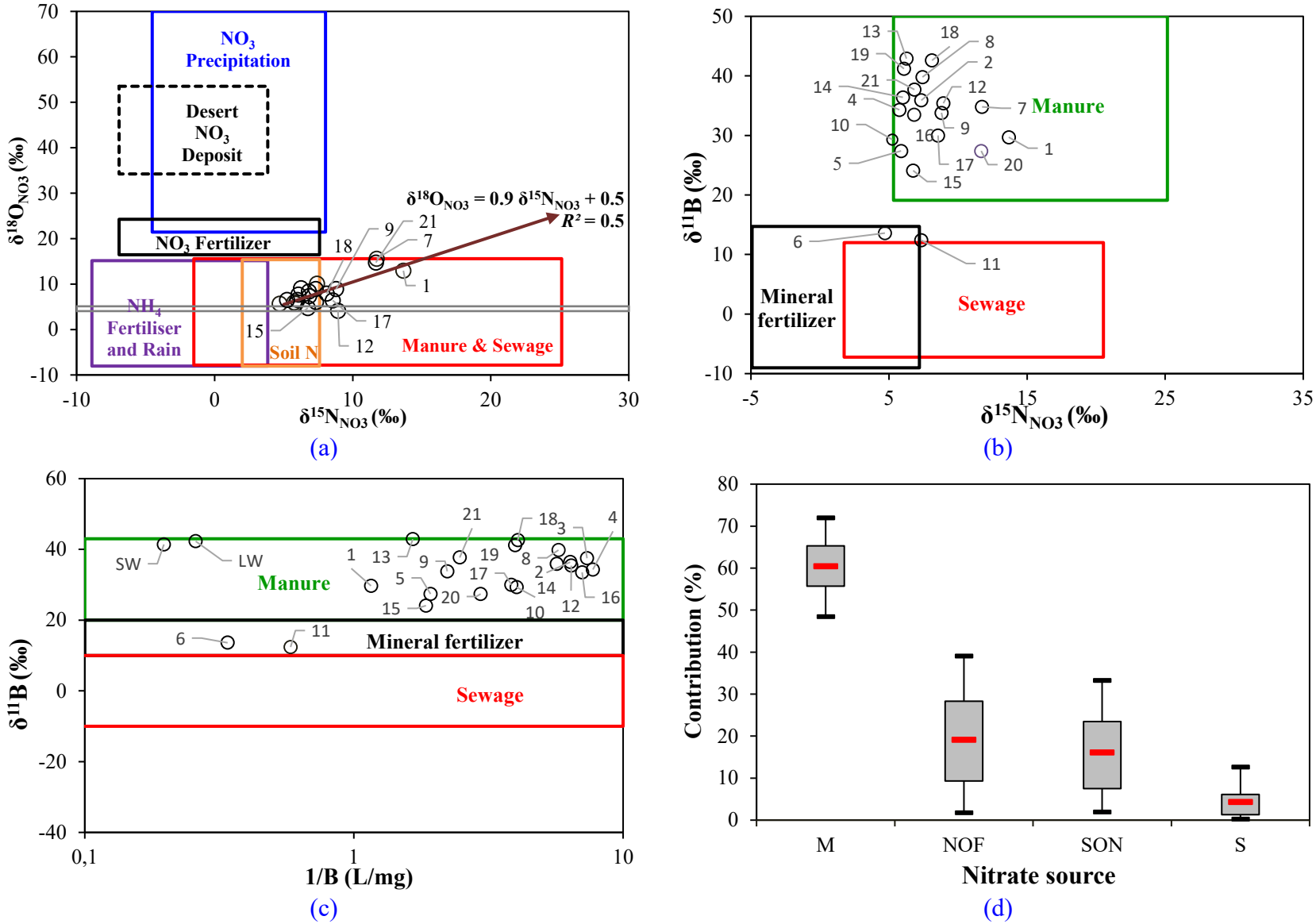

Figure 4. (a) Plot of $\delta^{15}N_{NO3}$ versus $\delta^{18}O_{NO3}$ values on Kendall diagram; (b) Plot of $\delta^{15}N_{NO3}$ versus $\delta^{11}B$ values; (c) Plot of B concentrations versus $\delta^{11}B$ values; and (d) apportionment of NO_3 sources based on the MixSIAR model (M: manure, NOF: NO_3 based fertilizers, SON: soil organic nitrogen, S: sewage). Boxplots illustrate the 25th, 50th, and 75th percentiles, while the whiskers indicate 5th and 95th percentiles.

5 Discussion

5.1 Water origin and influencing processes

The isotopic compositions of the groundwater samples are comparable to those from other studies undertaken on North-African Mediterranean coastal aquifers (Boumaiza et al., 2022a, 2020; Chafouq et al., 2018; Elmeknassi et al., 2022; Moussaoui et al., 2023). Furthermore, the groundwater isotopic compositions are comparable to the local weighted isotopic mean of wet season precipitation ($\delta^{18}O_{H2O} = -4.7‰$, and $\delta^{2}H_{H2O} = -26.1‰$) (Ben Ammar et al., 2020), suggesting that the OGM aquifer is mainly recharged by meteoric precipitation during the wet season, consistent with the fact that most precipitation occurs during the wet period from October to April in the study region. Most of $\delta^{18}O_{H2O}$ and $\delta^{2}H_{H2O}$ values plot along the GMWL (Craig, 1961) and the WMMWL (Celle, 2000) in Figure 5, suggesting that groundwater is mainly recharged through direct infiltration of meteoric recharge. The hydrogeological characteristics of the study area, i.e., an unconfined granular aquifer with a transmissivity of about $1\text{-}9\times10^{-4}$ m^2/s (Ben Ammar et al., 2016), are supportive of this conclusion.

Since substantial agricultural and irrigation activities occur across the study area, hydrogen and oxygen isotope fractionation affecting infiltrating water due to evaporation is expected if irrigation water-return flow is a significant source of recharge (Clark and Fritz, 1997; Harvey and Sibray, 2001; Mahlknecht et al., 2008). There is a decreasing trend of *d*-excess values against the increase of $\delta^{18}O_{H2O}$ values (Supplementary Figure S1a), suggesting evaporation influence (Deshpande et al., 2013; Lao et al., 2022a, 2023). However, most of groundwater samples (n = 17/21) have *d*-excess values >10‰, which is too high to justify the dominance of evaporation effect, rather, the influence of mixing with

continental runoff (*d*-excess ~10‰) is suggested (Santoni et al., 2018). The $\delta^{18}O_{H2O}$ values display little variability (with values of −4.9±0.5‰) across the groundwater samples with a wide range of measured TDS values (629-4,280 mg/L) (Supplementary Figure S1b). This suggests that evaporation is not the dominant process that increases groundwater salinity (Jia et al., 2017; Torres-Martínez et al., 2021). Rather, the increase in TDS appears to be caused by mixing with seawater. This notion is supported by the fact that the groundwater isotopic data plot along a line directed towards the isotopic composition of Mediterranean Sea and GEM Lagoon water (Figure 5). The water samples collected from the GEM Lagoon and from the Mediterranean Sea plot below the WMMWL and exhibit a low *d*-excess value (−1.1‰) (Figure 5; Supplementary Table S1). These observations indicate heavy isotope enrichment due to evaporative isotope fractionation effects and indicates the source water for the GEM Lagoon is from mixing with the Mediterranean Sea.

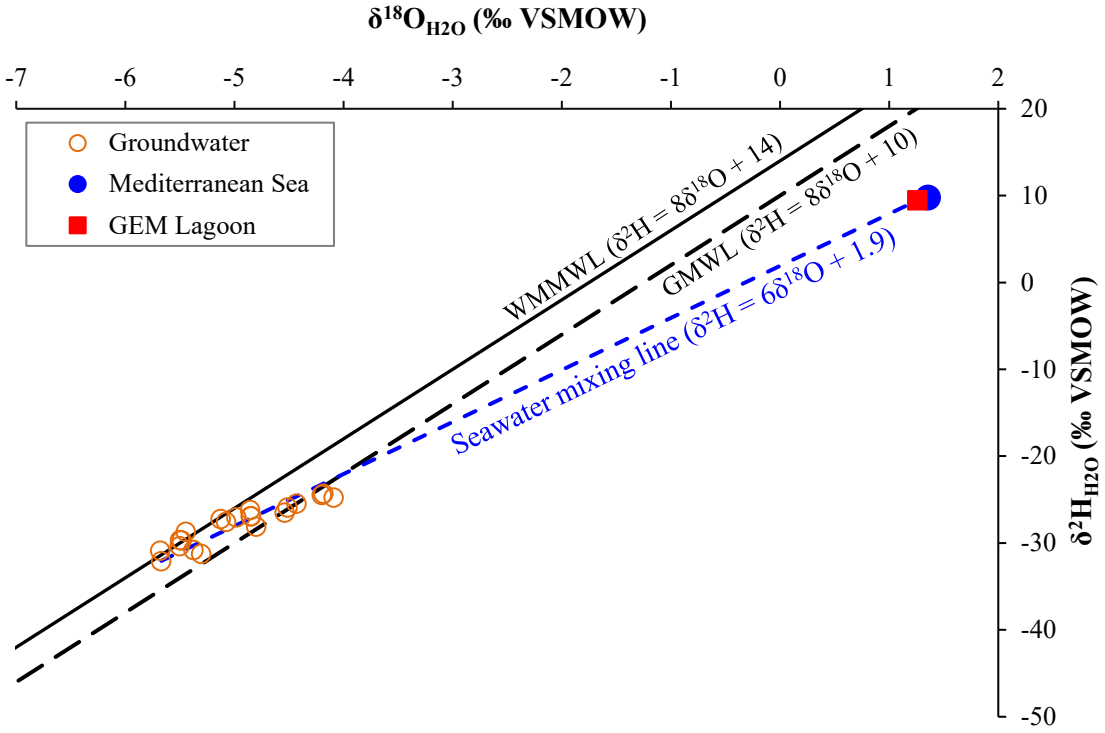

Figure 5. Distribution of isotopic values of water samples including groundwaters, surface water from GEM Lagoon, and surface water from the Mediterranean Sea.

5.2 **Nitrate origin in groundwater system**

All the measured NO_3 concentrations in the groundwater samples exceed the natural baseline threshold value of 3 mg/L (Ogrinc et al., 2019; Zendehbad et al., 2019), suggesting anthropogenic contamination in the study area, with 71% of the NO_3 concentrations in groundwater exceeding the drinking water limit. The finding from diagnostic plots (Figure 4) that manure is the dominant source of the elevated NO_3 concentrations in these groundwaters is consistent with land use within the OGM plain. Specifically, the OGM plain is a traditional agricultural area with a long history of intense fertilization/cultivation/irrigation activities. Manure-derived NO_3 in the groundwater appears to be linked to the excessive use of animal manure, which is applied as fertilizer for crops in agricultural areas, as well as manure that accumulates on the ground surface at local animal farms (Ben Ammar et al., 2016; Carrubba, 2017). Furthermore, these agricultural activities result in the accumulation of soil organic nitrogen and the subsequent formation of NO_3 from manure-based fertilizers infiltrating into the groundwaters as revealed by the quantified NO_3 contributions from manure, NOF, and SON (Figure 4d). Infiltrating rainwater and irrigation return flow contribute to the leaching of NO_3 from fertilizers and their by-products, which is then transported into the underlying groundwater system (Malki et al., 2017; Zhang et al., 2014). The occurrence of leaching fertilizers is supported by the positive correlation (R^2=0.5) between groundwater NO_3 concentrations and $\delta^{18}O_{H2O}$ values for some groundwater samples (Supplementary Figure S1c) with manure-derived contributions (60.4%) dominating over synthetic fertilizers (19.1%) according to the MixSIAR model. However, the contribution of synthetic fertilizers to NO_3

501 in groundwater is relatively high compared to other Mediterranean agricultural areas,
502 where contributions range between 8 and 15% (Boumaiza et al., 2022a, 2022b).

503 Elevated NO_3 concentrations (>150 mg/L, Figure 3) are observed in groundwater
504 down hydrogeologic gradient of the rural communities, suggesting that the minor sewage
505 contribution revealed by MixSIAR model is potentially from residences using inadequate
506 private sanitation systems (Ben Ammar et al., 2016; Carrubba, 2014). While efficient
507 private sanitation systems have a closed septic tank connected to a seepage distribution
508 field (MDDELCC, 2015), many private sanitations systems in North-Africa rely on a
509 unique open-bottom tank through which human waste can directly seep into the subsurface
510 and reach groundwater (Boumaiza et al., 2021, 2019). Consequently, sewage-derived NO_3
511 in groundwater is likely from direct wastewater discharge or leakage from inadequate
512 private sanitation systems. Even though ~40% of private homes in the OGM area rely on
513 the use of private sanitation systems (Ben Ammar et al., 2016), the sewage contribution
514 quantified by MixSIAR is low (4%), whereas $\delta^{11}B$ values indicate negligible sewage
515 contributions towards NO_3 in the OGM groundwater system. It is likely that mixing of
516 sewage-sourced and manure-sourced NO_3 occurs within the OGM groundwater system
517 although the isotope data demonstrate the manure is chief source of NO_3 contamination. It
518 is also important to note that the present study relies on MixSIAR isotopic end-member
519 values from another similar cases study (Kaown et al., 2023), and therefore analysing the
520 isotopic end-member compositions of local sources is necessary to refine our estimates and
521 thus improve characterization of the local NO_3 sources.

522 The elevated NO_3 concentrations in samples collected locally from the GEM
523 Lagoon and the Mediterranean Sea, combined with $\delta^{11}B$-evidence of manure influence,

524 may reflect organic manure used as part of the Ramli agricultural systems distributed across
525 the banks of GEM Lagoon (Aissaoui, 2020). Also, it cannot be rule out that there are
526 potential groundwater-surface water interactions that allow transport of NO_3 from the
527 OGM groundwater system into the GEM Lagoon and the Mediterranean Sea (e.g.,
528 submarine groundwater discharge). NO_3 transport from the OGM groundwater system to
529 the GEM Lagoon is further supported by groundwater flow as it is directed from the OGM
530 aquifer towards the GEM Lagoon (Supplementary Figure S2). It would be interesting to
531 quantify the submarine groundwater discharge flux in future related/similar studies.

532 5.3 **Nitrate transformation processes in the OGM groundwater system**

533 The most common nitrogen transformation processes include nitrification and
534 denitrification, which are biogeochemical processes mostly inherent to shallow
535 groundwater systems that are dependent on redox conditions (Gutiérrez et al., 2018).
536 During the denitrification process, ^{15}N and ^{18}O become progressively enriched in the
537 remaining NO_3, and $\delta^{15}N_{NO3}$ and $\delta^{18}O_{NO3}$ values in the remaining NO_3 pool increase as the
538 NO_3 concentration decreases (Kendall et al., 2007). Hence, the dual isotope plot of $\delta^{15}N_{NO3}$
539 versus $\delta^{18}O_{NO3}$ reveals that if microbial denitrification occurs in groundwater, it will
540 manifest as a positive slope of 0.5 or higher on the trendline between $\delta^{15}N_{NO3}$ and $\delta^{18}O_{NO3}$
541 values of NO_3 (Böttcher et al., 1990; Chen et al., 2009; Chen and MacQuarrie, 2005;
542 Fukada et al., 2004; Singleton et al., 2007). In Figure 4a, the plot of $\delta^{15}N_{NO3}$ against $\delta^{18}O_{NO3}$
543 values shows a positive slope of 0.9 suggesting that denitrification appears to occur in the
544 OGM groundwater system. However, denitrification cannot be the only biogeochemical
545 processes responsible for decreases in NO_3 concentrations because the correlation between
546 $\delta^{15}N_{NO3}$ values and NO_3 concentrations is weak (R^2 = 0.03, Supplementary Figure S1d).

547 Nevertheless, because most groundwater samples (n = 19/20) have positive $\Delta\delta^{18}O_{NO3}$
548 values ranging from +1.2 to +10.7‰ (Supplementary Table S1), the $\delta^{18}O_{NO3}$ data are also
549 consistent with denitrification occurring within the OGM groundwater system. On the
550 other hand, because some of groundwater samples plot within/near the expected theoretical
551 interval of $\delta^{18}O_{NO3}$ that ranges from 4.0 to 5.1‰ (Figure 4a; Supplementary Table S1),
552 nitrification must also be occurring within the OGM groundwater system.
553 Dissolved oxygen measured in groundwater samples from the study area ranges
554 from undetected to 7 mg/L (Supplementary Table S1). Hence, the DO concentrations in
555 groundwater samples with values >4 mg/L would tend to limit denitrification (Nikolenko
556 et al., 2018), which is not expected in highly oxygenated groundwaters. However,
557 denitrification could occur at anoxic sub-regions along the flow-paths and not necessarily
558 at the sampling locations. The plot of DO concentrations against pH values (Supplementary
559 Figure S1e) shows that groundwater samples #7, #8, #10, #12, and #13 (with measured DO
560 concentrations ranging from 0.2 to 3.3 mg/L) fall into the optimal denitrification zone,
561 suggesting that these samples are undergoing denitrification potentially under partially
562 oxidized conditions. In Figure S1e, groundwater samples #2, #9, #14, #16, and #21 plot
563 within the optimum nitrification zone suggesting NO_3 may reflect nitrification whereby
564 potential partial nitrification contributed an estimated of 76, 57, 71, 50, and 57%,
565 respectively, (Supplementary Table S1). The $\Delta\delta^{18}O_{NO3}$ values for samples #1 (8.9‰), #7
566 (10.8‰), and #21 (10.3‰) are high due to elevated measured $\delta^{18}O_{NO3}$ values, which range
567 from 11.7 to 13.7‰. This suggests that denitrification is taking place in the aquifer yielding
568 groundwater at wells #1, #7, and #21. However, sample #21 also falls within the optimal
569 nitrification zone due to its elevated DO concentration (Supplementary Figure S1e), even

570 though it has similar NO_3 isotopic values to that of sample #7 (Figure 4a). All the above
571 observations support that both denitrification and nitrification are important geochemical
572 processes of the nitrogen cycle within the OGM groundwater system.

573 # 6 Conclusion

574 The present study combined multiple environmental isotopic tracers ($\delta^{18}O_{H2O}$, $\delta^{2}H_{H2O}$,
575 $\delta^{15}N_{NO3}$, $\delta^{18}O_{NO3}$, and $\delta^{11}B$) with a Bayesian isotope MixSIAR model to distinguish NO_3
576 sources and their relative contributions; and to identify potential NO_3 transformation
577 processes in a coastal aquifer located in Tunisia. All collected groundwater samples from
578 the Mediterranean OGM coastal agricultural plain have NO_3 concentrations exceeding the
579 threshold of anthropogenic inputs, and most NO_3 concentrations in groundwater are above
580 the drinking water limit of 50 mg/L. The isotopic composition of NO_3 revealed different
581 anthropogenic sources contribute to NO_3 contamination of the local groundwater with
582 manure, sewage, and soil organic as the potential NO_3 sources. Nonetheless, the $\delta^{11}B$
583 values indicate that NO_3 is chiefly derived from manure. The Bayesian isotope MixSIAR
584 model results support manure as the major source of NO_3 to these groundwaters. The
585 present study highlights the usefulness of $\delta^{11}B$ to separate nitrate and other contaminants
586 from sewage and manure, because $\delta^{15}N_{NO3}$ and $\delta^{18}O_{NO3}$ values are commonly not capable
587 of differentiating these sources and are often masked by various simultaneously occurring
588 NO_3 transformation processes. Evidence of denitrification and nitrification are observed
589 with heterogenous occurrence/distribution within the OGM groundwater system, reflecting
590 the complexity of the study area, which is also influenced by seawater intrusion.

591 The measured NO_3 concentrations in the collected groundwater samples are two
592 times higher than that measured previously in 2010. This suggests the existence of

593 continuous sources of NO_3 that are deteriorating groundwater quality in the OGM aquifer.
594 Adaptation and mitigation strategies are required to improve the groundwater quality in the
595 future. Optimization strategies, including an introduction of environmentally safe
596 agricultural practices and an implementation of regulations for managing wastewater, are
597 encouraged to achieve a sustainable management of this economically strategic agricultural
598 area. The present study highlights the elevated NO_3 concentrations measured in the GEM
599 Lagoon with potential contribution of NO_3 via interactions between groundwater of the
600 OGM aquifer and surface water of the GEM Lagoon. This issue is of particular importance
601 because input of nutrients to the GEM Lagoon can lead to eutrophication limiting its
602 biodiversity.

603 **Acknowledgements**

604 The authors thank the Natural Sciences and Engineering Research Council of Canada for
605 funding this project through NSERC Discovery Grants RGPIN-07117 and RGPIN-03766
606 held by Prof. Romain Chesnaux and Prof. Bernhard Mayer, respectively. The authors thank
607 the local population of the OGM region who offered free access to their private wells during
608 fieldwork. The authors would like to thank Mr. Mohamed Khwatmia from the National
609 Center for Nuclear Sciences and Technologies (Tunisia) for his much-appreciated help
610 during fieldwork. Ms. Stefanie Schmidt is thanked for her assistance in performing the
611 chemical analyses at the Technical University of Darmstadt in Germany.

612

613 **References**
614
615 Aissaoui, A., 2020. Sowing seeds in Tunisian sands. Food and Agriculture Organization of
616 United Nations (www.fao.org/fao-stories/article/en/c/1287893/).
617 Aravena, R., Mayer, B., 2010. Isotopes and processes in the nitrogen and sulfur cycles, in:
618 Environmental Isotopes in Biodegradation and Bioremediation. pp. 203–246.
619 Ayache, F., Thompson, J.R., Flower, R.J., Boujarra, A., Rouatbi, F., Makina, H., 2009.
620 Environmental characteristics, landscape history and pressures on three coastal
621 lagoons in the Southern Mediterranean Region: Merja Zerga (Morocco), Ghar El
622 Melh (Tunisia) and Lake Manzala (Egypt). Hydrobiologia 622, 15–43.
623 Ben Ammar, S., Taupin, J.D., Ben Alaya, M., Zouari, K., Patris, N., Khouatmia, M., 2020.
624 Using geochemical and isotopic tracers to characterize groundwater dynamics and
625 salinity sources in the Wadi Guenniche coastal plain in northern Tunisia. J. Arid
626 Environ. 178, 1–14.
627 Ben Ammar, S., Taupin, J.D., Zouari, K., Khouatmia, M., 2016. Identifying recharge and
628 salinization sources of groundwater in the Oussja Ghar el Melah plain (northeast
629 Tunisia) using geochemical tools and environmental isotopes. Environ. Earth Sci.
630 75, 1–16.
631 Blarasin, M., Cabrera, A., Ioannis Matiatos, I., Becher Quinodóz, F., Giuliano Albo, J., Lutri,
632 V., Matteoda, E., Panarello, H., 2020. Comparative evaluation of urban versus
633 agricultural nitrate sources and sinks in an unconfined aquifer by isotopic and
634 multivariate analyses. Sci. Total Environ. 741, 1–15.
635 Blarasin, M., Cabrera, A., Matteoda, E., 2014. Aguas subterráneas de la provincia de
636 Córdoba, Argentina. UniRío. Río Cuarto.
637 Böttcher, J., Strebel, O., Voerkelius, S., Schmidt, H.L., 1990. Using isotope fractionation of
638 nitrate-nitrogen and nitrate-oxygen for evaluation of microbial denitrification in a
639 sandy aquifer. J. Hydrol. 114, 413–424.
640 Bouchouicha, S., 2004. Étude Hydrogéologique de la Nappe Utique-Aousja. Vulnérabilité
641 et établissement des Périmètres de Protection. Mémoire de Maitrise, Université de
642 Bizerte, Bizerte, Tunisie.
643 Boumaiza, L., Chabour, N., Drias, T., 2019. Reviewing the potential anthropogenic sources
644 of groundwater contamination - Case study of the expanding urban area of Taleza
645 in Algeria, in: Proceedings of the 72nd Canadian Geotechnical Conference (GeoSt-
646 John's 2019), Saint-John's, Newfoundland and Labrador, Canada,. p. 9.
647 Boumaiza, L., Chesnaux, R., Drias, T., Walter, J., Huneau, F., Garel, E., Knoeller, K.,
648 Stumpp, C., 2020. Identifying groundwater degradation sources in a Mediterranean
649 coastal area experiencing significant multi-origin stresses. Sci. Total Environ. 746,
650 1–20.
651 Boumaiza, L., Chesnaux, R., Walter, J., Drias, T., Huneau, F., Garel, E., Vystavna, Y.,
652 Stumpp, C., 2021. Reviewing the anthropogenic sources of groundwater
653 contamination in the Plain of the El-Nil River, Algeria, in: Proceedings of the 74th
654 Canadian Geotechnical Conference and the 14th Joint CGS/IAH-CNC
655 Groundwater Conference (GeoNiagara-2021), Niagara Falls, Ontario, Canada. p. 9.
656 Boumaiza, L., Walter, J., Chesnaux, R., Huneau, F., Garel, E., Erostate, M., Johannesson,
657 K.H., Vystavna, Y., Bougherira, N., Bordeleau, G., Stotler, R.L., Blarasin, M.,
658 Gutierrez, M., Knöller, K., Stumpp, C., 2022a. Multi-tracer approach to understand

659 nitrate contamination and groundwater-surface water interactions in the
660 Mediterranean coastal area of Guerbes-Senhadja, Algeria. J. Contam. Hydrol. 251,
661 1–16.
662 Boumaiza, L., Walter, J., Chesnaux, R., Zahi, F., Huneau, F., Garel, E., Stotler, R.L.,
663 Bordeleau, G., Drias, T., Johannesson, K.H., Vystavna, Y., Re, V., Knöller, K.,
664 Stumpp, C., 2022b. Combined effects of seawater intrusion and nitrate
665 contamination on groundwater in coastal agricultural areas: A case from the Plain
666 of the El-Nil River (North-Eastern Algeria). Sci. Total Environ. 851, 1–13.
667 Bouzourra, H., Bouhlila, R., Elango, L., Slama, F., Ouslati, N., 2015. Characterization of
668 mechanisms and processes of groundwater salinization in irrigated coastal area
669 using statistics, GIS, and hydrogeochemical investigations. Environ. Sci. Pollut.
670 Res. 22, 2643–2660.
671 Brookfield, A.E., Hansen, A.T., Sullivan, P.L., Czuba, J.A., Kirk, M.F., Li, L., Newcomer,
672 M.E., Wilkinson, G., 2021. Predicting algal blooms: Are we overlooking
673 groundwater? Sci. Total Environ. 769, 1–15.
674 Burrolet, P.F., Dumon, E., 1952. Geological map of Porto Farina. National Office of Mines,
675 Tunisia.
676 Cao, S., Fei, Y., Tian, X., Cui, X., Zhang, X., Yuan, R., Li, Y., 2021. Determining the
677 origin and fate of nitrate in the Nanyang Basin, Central China, using environmental
678 isotopes and the Bayesian mixing model. Environ. Sci. Pollut. Res. 28, 48343–48361.
679 Carrubba, S., 2017. Cartographie des vulnérabilités de l'aquifère côtier de Ghar El Melh en
680 Tunisie. Strategic Partnership for the Mediterranean Sea Large Marine Ecosystem
681 (MedPartnership), Project Report.
682 Carrubba, S., 2014. Vulnerability mapping of the Ghar El Melh coastal aquifer in Tunisia.
683 Strategic Partnership for the Mediterranean Sea Large Marine Ecosystem
684 (MedPartnership), Project Report.
685 Casciotti, K.L., Sigman, D.M., Hastings, M.G., Böhlke, J.K., Hilkert, A., 2002.
686 Measurement of the oxygen isotopic composition of nitrate in seawater and
687 freshwater using the denitrifier method. Anal. Chem. 74, 4905–4912.
688 Celle, H., 2000. Caractérisation des précipitations sur le pourtour de la Méditerranée
689 occidentale. Approche isotopique et chimique. PhD thesis, Université d'Avignon,
690 France.
691 Chafouq, D., El Mandour, A., Elgettafi, M., Himi, M., Chouikri, I., Casas, A., 2018.
692 Hydrochemical and isotopic characterization of groundwater in the Ghis-Nekor
693 plain (northern Morocco). J. African Earth Sci. 139, 1–13.
694 Chelbi, F., Paskoff, R., Trousset, P., 1995. La baie d'Utique et son évolution depuis
695 l'Antiquité: une réévaluation géoarchéologique. Antiq. africaines 31, 7–51.
696 Chen, D.J.Z., MacQuarrie, K.T.B., 2005. Correlation of δ15N and δ18O in NO3−during
697 denitrification in groundwater. J. Environ. Eng. Sci. 4, 221–226.
698 Chen, F., Jia, G., Chen, J., 2009. Nitrate Sources and Watershed Denitrification Inferred
699 from Nitrate Dual Isotopes in the Beijiang River, South China. Biogeochemistry,
700 94, 163-174.
701 Chesnaux, R., Marion, D., Boumaiza, L., Richard, S., Walter, J., 2021. An analytical
702 methodology to estimate the changes in fresh groundwater resources with sea-level
703 rise and coastal erosion in strip-island unconfined aquifers: illustration with Savary
704 Island, Canada. Hydrogeol. J. 29, 1355–1364.

Clark, I.D., Fritz, P., 1997. Environmental isotopes in hydrogeology. CRC Press-Lewis Publishers.
Craig, H., 1961. Isotopic variations in meteoric waters. Science (80-.). 133, 1702–1703.
Dansgaard, W. (1964) Stable isotopes in precipitation. *Tellus* 16(4), 436–468.
Deshpande, R.D., Muraleedharan, P.M., Singh, R.L., Kumar, B., Rao, M.S., Dave, M., Sivakumar, K.U., Gupta, S.K. 2013. Spatio-temporal distributions of δ18O, δD and salinity in the Arabian Sea: Identifying processes and controls, Marine Chemistry, 157, 144-161.
Elmeknassi, M., Bouchaou, L., El Mandour, A., Elgettafi, M., Himi, M., Casas, A., 2022. Multiple stable isotopes and geochemical approaches to elucidate groundwater salinity and contamination in the critical coastal zone: A case from the Bou-areg and Gareb aquifers (North-Eastern Morocco). Environ. Pollut. 300, 1–13.
Erostate, M., Huneau, F., Garel, E., Lehmann, M.F., Kuhn, T., Aquilina, L., Vergnaud-Ayraud, V., Labasque, T., Santoni, S., Robert, S., Provitolo, D., Pasqualini, V., 2018. Delayed nitrate dispersion within a coastal aquifer provides constraints on land-use evolution and nitrate contamination in the past. Sci. Total Environ. 644, 928–940.
Fukada, T., Hiscock, K.M., Dennis, P.F., 2004. A dual-isotope approach to the nitrogen hydrochemistry of an urban aquifer. Appl. Geochemistry. https://doi.org/10.1016/j.apgeochem.2003.11.001
Gaillardet, J., Lemarchand, D., Göpel, C., G., M., 2001. Evaporation and sublimation of boric acid: application for boron purification from organic rich solutions. Geostand. Newsl. 25, 67–75.
Gomez Isaza, D.F., Cramp, R.L., Franklin, C.E., 2020. Living in polluted waters: A meta-analysis of the effects of nitrate and interactions with other environmental stressors on freshwater taxa. Environ. Pollut. 261, 1–12.
Guerrot, C., Millot, R., Robert, M., Negrel, P., 2011. Accurate and High-Precision Determination of Boron Isotopic Ratios at Low Concentration by MC-ICP-MS (Neptune). Geostand. Geoanalytical Res. 35, 275–284.
Gutiérrez, M., Biagioni, R.N., Alarcòn-Herrera, M.T., Rivas-Lucero, B.A., 2018. An overview of nitrate sources and operating processes in arid and semiarid aquifer systems. Sci. Total Environ. 624, 1513–1522.
Harvey, F.E., Sibray, S.S., 2001. Delineating Ground Water Recharge from Leaking Irrigation Canals Using Water Chemistry and Isotopes. Groundwater 39, 408–421.
He, S., Li, P., Su, F., Wang, D., Ren, X., 2022. Identification and apportionment of shallow groundwater nitrate pollution in Weining Plain, northwest China, using hydrochemical indices, nitrate stable isotopes, and the new Bayesian stable isotope mixing model (MixSIAR). Environ. Pollut. 298, 1–11.
Hendry, M.J., McCready, R.G.L., Gould, W.D., 1984. Distribution, source and evolution of nitrate in a glacial till of southern Alberta, Canada. J. Hydrol. 70, 177–198.
Holloway, J.M., Dahlgren, R.A., 2002. Nitrogen in rock: Occurrences and biogeochemical implications. Global Biogeochem. Cycles 14, 1–17.
Jacks, G., Sharma, V.P., 1983. Nitrogen circulation and nitrate in groundwater in an agricultural catchment in southern India. Environ. Geol. 5, 61–64.
Jia, Y., Guo, H., Xi, B., Jiang, Y., Zhang, Z., Yuan, R., Yi, W., Xue, X., 2017. Sources of groundwater salinity and potential impact on arsenic mobility in the western Hetao

751 Basin. Sci. Total Environ. 601, 691–702.
752 Jin, Z., Qin, X., Chen, L., Jin, M., Li, F., 2015. Using dual isotopes to evaluate sources and
753 transformations of nitrate in the West Lake watershed, eastern China. J. Contam.
754 Hydrol. 177, 64–75.
755 Kaown, D., Koh, D.C., Mayer, B., Mahlknecht, J., Ju, Y., Rhee, S.K., Kim, J.H., Park, D.K.,
756 Park, I., Lee, H.L., Yoon, Y.Y., Lee, K.K., 2023. Estimation of nutrient sources and
757 fate in groundwater near a large weir-regulated river using multiple isotopes and
758 microbial signatures. J. Hazard. Mater. 446, 1–13.
759 Kendall, C., 1998. Tracing Nitrogen Sources and Cycling in Catchments. Isot. Tracers
760 Catchment Hydrol. 519–576.
761 Kendall, C., Elliott, E.M., Wankel, S.D., 2007. Tracing Anthropogenic Inputs of Nitrogen
762 to Ecosystems, Chapter 12, In: R.H. Michener and K. Lajtha (Eds.). Stable Isot.
763 Ecol. Environ. Sci. Second Ed. Blackwell Publ. 375–449.
764 Komor, S.C., 1997. Boron contents and isotopic composition of hog manure, selected
765 fertilizers, and water in Minnesota. J. Environ. Qual. 26, 1212–1222.
766 Kou, X., Ding, J., Li, Y., Li, Q., Mao, L., Xu, C., Zheng, Q., Zhuang, S. 2021. Tracing nitrate
767 sources in the groundwater of an intensive agricultural region, Agricultural Water
768 Management, 250, 1-10.
769 Kruk, M.K., Mayer, B., Nightingale, M., Laceby, J.P., 2020. Tracing nitrate sources with a
770 combined isotope approach (δ15NNO3, δ18ONO3 and δ11B) in a large mixed-use
771 watershed in southern Alberta. Sci. Total Environ. 703, 1–15.
772 Lane, A.D., Kirk, M.F., Whittemore, D.O., Stotler, R., Hildebrand, J., Feril, O., 2020. Long-
773 term (1970s–2016) changes in groundwater geochemistry in the High Plains aquifer
774 in south-central Kansas, USA. Hydrogeol. J. 28, 491–501.
775 Lao, Q., Zhang, S., Li, Z., Chen, F., Zhou, X., Jin, G., Huang, P., Deng, Z., Chen, C., Zhu,
776 Q., Lu, X. 2022a. Quantification of the seasonal intrusion of water masses and their
777 impact on nutrients in the Beibu Gulf using dual water isotopes. Journal of
778 Geophysical Research: Oceans, 127, e2021JC018065.
779 https://doi.org/10.1029/2021JC018065
780 Lao, Q., Wu, J., Chen, F., Zhou, X., Li, Z., Chen, C., Zhu, Q., Deng, Z., Li, J. 2022b,
781 Increasing intrusion of high salinity water alters the mariculture activities in
782 Zhanjiang Bay during the past two decades identified by dual water isotopes.
783 Journal of Environnemental Management, 320, 1-14.
784 Lao, Q., Lu, X., Chen, F., Jin, G., Chen, C., Zhou, X., Zhu, Q. 2023. Effects of upwelling
785 and runoff on water mass mixing and nutrient supply induced by typhoons: Insight
786 from dual water isotopes tracing, Limnology and Oceanography. 68, 284-295.
787 Lasagna, M., De Luca, D.A., 2017. Evaluation of sources and fate of nitrates in the western
788 Po plain groundwater (Italy) using nitrogen and boron isotopes. Environ. Sci.
789 Pollut. Res. 26, 2089–2104.
790 Mahlknecht, J., Horst, A., Hernández-Limón, G., Aravena, R., 2008. Groundwater
791 geochemistry of the Chihuahua City region in the Rio Conchos Basin (northern
792 Mexico) and implications for water resources management. Hydrol. Process. 22,
793 4736–4751.
794 Malki, M., Bouchaou, L., Hirich, A., Ait Brahim, Y., Choukr-Allah, R., 2017. Impact of
795 agricultural practices on groundwater quality in intensive irrigated area of Chtouka-
796 Massa, Morocco. Sci. Total Environ. 574, 760–770.

MAT, (Ministère de l'Agriculture de la Tunisie), 2006. Rapports techniques des piézomètres et des forages - Annuaires de surveillance piézométrique 1971-2006. inistère de l'Agriculture de la Tunisie, Tunisie.

Matiatos, I., 2016. Nitrate source identification in groundwater of multiple land-use areas by combining isotopes and multivariate statistical analysis: A case study of Asopos basin (Central Greece). Sci. Total Environ. 541, 802–814.

MDDELCC, (Ministère du Développement durable de l'Environnement et de la Lutte contre les changements climatiques), 2015. Guide technique sur le traitement des eaux usées des résidences isolées. Règlement sur l'évacuation des eaux usées des résidences isolées. Québec, Canada.

Melki, F., Zouaghi, T., Harrab, S., Casas Sainz, A., Bedir, M., Zargouni, F., 2011. Structuring and evolution of Neogene transcurrent basins in the Tellian foreland domain, north-eastern Tunisia. J. Geodyn. 52, 57–69.

Mills, T.J., Mast, M.A., Thomas, J., Keith, G., 2016. Controls on selenium distribution and mobilization in an irrigated shallow groundwater system underlain by Mancos Shale, Uncompahgre River Basin, Colorado, USA. Sci. Total Environ. 566–567, 1621–1631.

Moon, H.S., Komlos, J., Jaffé, P.R., 2007. Uranium reoxidation in previously bioreduced sediment by dissolved oxygen and nitrate. Environ. Sci. Technol. 41, 4587–4592.

Moore, K.B., Ekwurzel, B., Esser, B.K., Hudson, G.B., Moran, J.., 2006. Sources of groundwater nitrate revealed using residence time and isotope methods. Appl. Geochemistry 21, 1016–1029.

Moussaoui, I., Rosa, E., Cloutier, V., Neculita, C.M., Dassi, L., 2023. Chemical and isotopic evaluation of groundwater salinization processes in the Djebeniana coastal aquifer, Tunisia. Appl. Geochemistry 149, 1–13.

Nikolenko, O., Jurado, A., Borges, A.V., Knöller, K., Brouyère, S., 2018. Isotopic composition of nitrogen species in groundwater under agricultural areas: a review. Sci. Total Environ. 621, 1415–1432.

Ogrinc, N., Tamse, S., Zavadlav, S., Vrzel, J., Jin, L., 2019. Evaluation of geochemical processes and nitrate pollution sources at the Ljubljansko polje aquifer (Slovenia): a stable isotope perspective. Sci. Total Environ. 646, 1588–1600.

Ouerghi, S., 2021. A GIS-based Assessment of the Vulnerability to Potential Pollution of the Alluvial Aquifer of Aousja-Ghar El Melh (North-East of Tunisia) Using the Parametric Method DRASTIC. Eur. J. Eng. Technol. Res. 6, 81–87.

Parnell, A.C., Inger, R., Bearhop, S., Jackson, A.L., 2010. Source partitioning using stable isotopes: coping with too much variation. PLoS One 5(3):e9672. https://doi.org/10.1371/journal.pone.0009672

Penna, D., Stenni, B., Šanda, M., Wrede, S., Bogaard, T.A., Gobbi, A., Borga, M., Fischer, B.M.C., Bonazza, M., Chárová, Z., 2010. On the reproducibility and repeatability of laser absorption spectroscopy measurements for δ 2 H and δ 18 O isotopic analysis. Hydrol. Earth Syst. Sci. 14, 1551–1566.

Pimienta, J., 1959. Le cycle pliocène-actuel dans les bassins paraliques de Tunis. Mémoires de la Société Géologique de France, No. 85, Paris, France.

Puig, R., Soler, A., Widory, D., Mas-Pla, J., Domènech, C., Otero, N., 2017. Characterizing sources and natural attenuation of nitrate contamination in the BaixTer aquifer system (NE Spain) using a multi-isotope approach. Sci. Total Environ. 580, 518–

532.
Pulido-Bosch, A., Rigol-Sanchez, J.P., Vallejos, A., Andreu, J.M., Ceron, J.C., Molina-Sanchez, L., Sola, F., 2018. Impacts of agricultural irrigation on groundwater salinity. Environ. Earth Sci. 77, 1–14.
Re, V., Kammoun, S., Sacchi, E., Trabelsi, R., Zouari, K., Matiatos, I., Allais, E., Daniele, S., 2021. A critical assessment of widely used techniques for nitrate source apportionment in arid and semi-arid regions. Sci. Total Environ. 775, 1–12.
Re, V., Sacchi, E., 2017. Tackling the salinity-pollution nexus in coastal aquifers from arid regions using nitrate and boron isotopes. Environ. Sci. Pollut. Res. 24, 13247–13261.
Saadaoui, M., 1983. Note sur L'hydrologie du Lac de Ghar el Melh. Bureau de l'inventaire et de Recherches Hydrologiques, Tunisie.
Santoni, S., Huneau, F., GAREL, E., Celle-Jeanton, H., 2018. Multiple recharge processes to heterogeneous Mediterranean coastal aquifers and implications on recharge rates evolution in time. J. Hydrol. 559, 669–683.
Scanlon, B.R., Reedy, R.C., Bronson, K.F., 2008. Impacts of Land Use Change on Nitrogen Cycling Archived in Semiarid Unsaturated Zone Nitrate Profiles, Southern High Plains, Texas. Environ. Sci. Technol. 42, 1–7.
Schroeder, A., Souza, D.H., Fernandes, M., Rodrigues, E.B., Trevisan, V., Skoronski, E., 2020. Application of glycerol as carbon source for continuous drinking water denitrification using microorganism from natural biomass. J. Environ. Manage. 256, 109964–109971.
Sigman, D.M., Casciotti, K.L., Andreani, M., Barford, C., Galanter, M., Böhlke, J.K., 2001. A bacterial method for the nitrogen isotopic analysis of nitrate in seawater and freshwater. Anal. Chem. 73, 4145–4153.
Singleton, M.J., Esser, B.K., Moran, J.E., Hudson, G.B., Mcnab, W.W., Harter, T., 2007. Saturated zone denitrification: Potential for natural attenuation of nitrate contamination in shallow groundwater under dairy operations. Environ. Sci. Technol. 41, 759–765.
Stock, B.C., Jackson, A.L., Ward, E.J., Parnell, A.C., Phillips, D.L., Semmens, B.X., 2018. Analyzing mixing systems using a new generation of Bayesian tracer mixing models. PeerJ 6, e5096. https://doi.org/https://doi.org/10.7717/peerj.5096.
Sutton, M.A., Howard, C.M., Erisman, J.W., Billen, G., Bleeker, A., Grennfelt, P., Van Grinsven, H., Grizzetti, B., 2011. The European Nitrogen Assessment, The European Nitrogen Assessment. Cambridge University Press.
Torres-Martínez, J.A., Mora, A., Mahlknecht, J., Daessle, L.W., Cervantes-Aviles, P.A., Ledesma-Ruiz, R., 2021. Estimation of nitrate pollution sources and transformations in groundwater of an intensive livestock-agricultural area (Comarca Lagunera), combining major ions, stable isotopes and MixSIAR model. Environ. Pollut. 269, 1–12.
Vengosh, A., Heumann, K.G., Juraske, S., Kasher, R., 1994. Boron isotope application for tracing sources of contamination in groundwater. Environ. Sci. Technol. 28, 1968–1974.
Vystavna, Y., Diadin, D., Yakovlev, V., Hejzlar, J., Vadillo, I., Huneau, F., Lehmann, M.F., 2017. Nitrate contamination in a shallow urban aquifer in East Ukraine: evidence from hydrochemical, stable isotopes of nitrate and land use analysis. Environ. Earth

Sci. 76, 1–13.
Ward, M., Jones, R., Brender, J., De Kok, T., Weyer, P., Nolan, B., Van Breda, S., 2018. Drinking water nitrate and human health: an updated review. Int. J. Environ. Res. Public Health 15, 1–31.
Weeks, E.P., McMahon, P.B., 2007. Nitrous Oxide Fluxes from Cultivated Areas and Rangeland: U.S. High Plains. Vadose Zo. J. 6, 496–510.
WHO, (World Health Organization), 2017. Guidelines for drinking-water quality, 4th edition, incorporating the 1st addendum. ISBN: 978-92-4-154995-0.
Yeshno, E., Arnon, S., Dahan, O., 2019. Real-time monitoring of nitrate in soils as a key for optimization of agricultural productivity and prevention of groundwater pollution. Hydrol. Earth Syst. Sci. 23, 3997–4010.
Zendehbad, M., Cepuder, P., Loiskandl, W., Stumpp, C., 2019. Source identification of nitrate contamination in the urban aquifer of Mashhad, Iran. J. Hydrol. Reg. Stud. 25, 1–14.
Zhang, Y., Li, F., Zhang, Q., Li, J., Liu, Q., 2014. . Tracing nitrate pollution sources and transformations in surface- and ground-waters using environmental isotopes. Sci. Total Environ. 490, 213–222.